American Mineralogist, Volume 79, pages 73–79, 1994

Twinning in meteoritic and synthetic perovskite

LINDSAY P. KELLER,* PETER R. BUSECK
Departments of Geology and Chemistry, Arizona State University, Tempe, Arizona 85287-1404, U.S.A.

ABSTRACT

Transmission electron microscope observations of end-member perovskite from two carbonaceous chondrite meteorites show that fine-scale twinning is common. Three twin laws are observed: (1) a 90° rotation around [101], (2) a 180° rotation around [101], and (3) a 180° rotation around [121]. The meteoritic perovskite is predominantly twinned according to 3 above, in contrast to terrestrial perovskites, in which operations 1 and 2 are more common. Twinning on (121) [pseudocubic (111)] occurs during cooling through the cubic-orthorhombic phase transition.

Experiments on synthetic perovskite indicate that twinning on (121) is the predominant twin law observed in material that was cooled rapidly (>50 °C/min). In experiments using slower cooling rates, (101) twins are more prevalent than (121) twins. These results indicate that meteoritic perovskite displaying (121) twins was heated to temperatures above the cubic-orthorhombic phase transition (~1573 K) and rapidly cooled. This constraint strongly limits the mechanism responsible for the formation of perovskite in these meteorites.

INTRODUCTION

The perovskite structure is of great importance, both for understanding mantle geophysics (e.g., Williams et al., 1987) and in certain technological applications such as ferroelectrics and superconductors (e.g., Newnham, 1987). The microstructures of compounds with the perovskite structure have been widely studied by electron microscopy, but only a few investigations have considered the microstructures in end-member perovskite (e.g., Doukhan and Doukhan, 1986; Hu et al., 1992). End-member perovskite is rare in terrestrial rocks; perovskite usually shows substantial solid solution with incompatible elements, typically large rare earth elements (La and Ce), Na, and Nb, which accounts for varietal names such as loparite and dysanalite. The few occurrences of near end-member perovskite are restricted to metamorphic rocks that have undergone deformation. Thus, it is difficult to differentiate microstructures arising from deformation events from those resulting from phase transitions. In some carbonaceous chondrite meteorites, however, we have the opportunity to study essentially pure $CaTiO_3$ perovskite from undeformed rocks.

We report here on our transmission electron microscope (TEM) studies of microstructures in meteoritic perovskite. Perovskite ($CaTiO_3$) is a common accessory mineral in Ca- and Al-rich refractory inclusions (CAIs) in some carbonaceous chondrite meteorites. Much of this perovskite occurs in refractory rims, where it is intergrown with other high-temperature minerals, mainly spinel and hibonite. Isotope and trace-element studies indicate that these refractory rims are evaporative residues from a high-temperature flash-heating event early in the history of our solar system (Boynton and Wark, 1987; Wark et al., 1988). However, major uncertainties exist regarding the thermal history of these refractory rims; these uncertainties include the maximum temperature attained and the relative heating and cooling rates that the inclusions experienced. The occurrence and structural characteristics of end-member perovskite provide information regarding the origin of refractory rims on CAIs.

Ideal perovskite is cubic, space group $Pm3m$, with a = ~0.382 nm. The structure consists of corner-sharing TiO_6 octahedra that form a regular three-dimensional framework, with Ca occupying the large cuboctahedral sites formed by the octahedra (Fig. 1a). At room temperature, Ca is slightly too small for its site, causing the TiO_6 octahedra to tilt and rotate slightly (Fig. 1b), thereby reducing the symmetry from cubic to orthorhombic (Sasaki et al., 1987). The orthorhombic unit cell (denoted by the subscript o) is related to the pseudocubic subcell (subscript c) by the following relations: $a_o = \sqrt{2}a_c$, $b_o = 2a_c$, and $c_o = \sqrt{2}a_c$. We use the standard space group setting for orthorhombic perovskite, *Pnma*.

It is well known that a reversible transition occurs in $CaTiO_3$ between high-temperature cubic symmetry and low-temperature orthorhombic symmetry (e.g., Megaw, 1973; Müller and Roy, 1974; Liu and Liebermann, 1988; Liebermann et al., 1990). However, uncertainties exist regarding the nature of the transition from cubic to orthorhombic symmetry, as well as the nature of the transition mechanism. A consequence of the cubic to orthorhombic transition mechanism is the development of microtwinning on the major pseudocubic axes as the

* Present address: MVA, Inc., 5500 Oakbrook Parkway, Suite 200, Norcross, Georgia 30093, U.S.A.

0003–004X/94/0102–0073$02.00

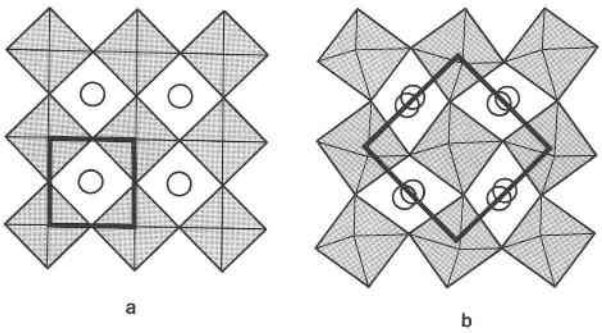

Fig. 1. (a) A [010] projection of the ideal cubic perovskite structure (space group $Pm3m$). The shaded squares are the TiO_6 octahedra, and the open circles represent Ca atoms. A unit cell is outlined in bold lines. (b) A [010] projection of the orthorhombic perovskite structure (space group $Pnma$).

structure loses symmetry on cooling through the transition temperature.

Experimental

We studied perovskite from type A and type B CAIs from the Allende meteorite, and a single type A inclusion from the Vigarano CV3 carbonaceous chondrite (the reader is referred to the review paper of Grossman, 1980, for a summary of CAI classification). The perovskite occurs as rounded, isolated grains that are typically <10 μm in size but average about 1–2 μm in diameter (Fig. 2). Quantitative energy-dispersive X-ray analyses of the perovskites show no detectable elements other than Ca and Ti. A total of six regions of interest were extracted from polished thin sections, attached to Cu grid supports, and ion thinned to electron transparency using 5-kV Ar ions. From these specimens, we were able to study over 50 perovskite grains.

Cooling-rate experiments were performed using synthetic perovskite prepared by sintering pellets of stoichi-

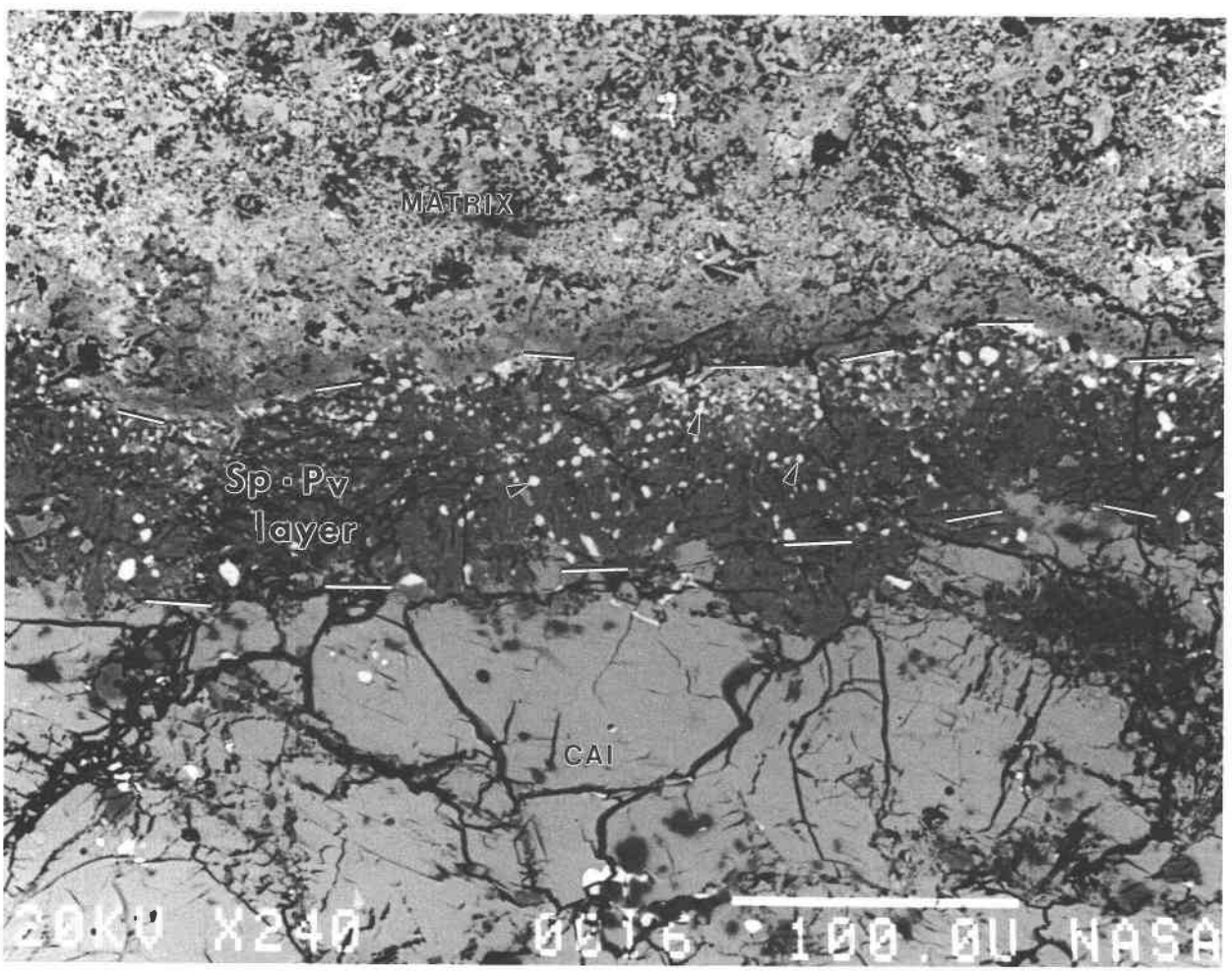

Fig. 2. Backscattered scanning electron microscope image of a portion of a Ca- and Al-rich inclusion from the Allende meteorite showing the size and distribution of perovskite (Pv) grains in our sample.

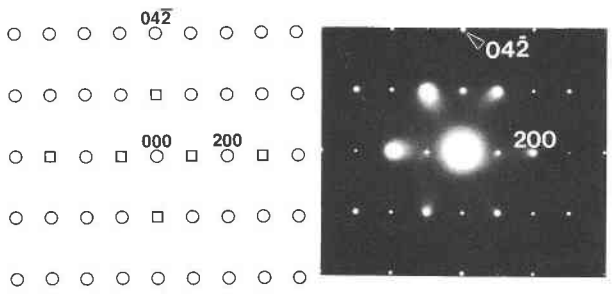

Fig. 3. Schematic and SAED patterns of the [012] zone. The open circles are the allowed reflections, and the open squares designate forbidden reflections that are generated by multiple diffraction.

ometric mixtures of reagent grade $CaCO_3$ and TiO_2 in air at 1773 K for 48 h. The pellets were then ground in an agate mortar and pestle, repelletized, and heated at 1973 K for 24 h. X-ray powder diffraction patterns contain only the sharp peaks of perovskite; no peaks from impurity phases were observed. For the cooling-rate experiments, 50-mg to 100-mg samples of powdered $CaTiO_3$ were loaded into Pt capsules and suspended in a sealed vertical-tube furnace, equilibrated at 1873 K, and cooled to 1073 K at 10, 50, and 100 °C/min, and then drop quenched. Aliquots of the synthetic material were prepared for TEM observation by grinding the sample in acetone and dispersing it onto holey carbon thin films attached to Cu grids. High-resolution images and electron diffraction patterns were obtained using JEOL 2000FX (200 kV) and JEOL 4000EX (400 kV) transmission electron microscopes (TEM). Optical diffractograms of small regions in high-resolution TEM images were recorded on an optical bench.

Twinning

Twinning is well developed and common in the perovskite grains we studied. We observed twinning according to three twin laws: (1) a 90° rotation around [101], (2) a 180° rotation around [101], and (3) a 180° rotation around [121]. Only the first two operations are common in natural terrestrial perovskites (White et al., 1985; Hu et al., 1992). Although [121] twinning has been identified in perovskite heated to high temperatures (Liebermann et al., 1990) and in several terrestrial perovskites, it is apparently poorly developed and rare in end-member perovskite (Kay and Bailey, 1957; White et al., 1985; Hu et al., 1992). The meteoritic perovskite that we studied typically shows fine-scale twinning by a 180° rotation around [121], which is in contrast to terrestrial perovskites, where (101) twins predominate.

The 180° rotation twin around [121]

The [012] zone of orthorhombic perovskite corresponds to the [111] zone of the cubic subcell and shows a strong pseudohexagonal symmetry. Figure 3 shows an experimental selected-area electron diffraction (SAED) pattern together with a schematic diffraction pattern for the [012] zone. Because of the thickness of the perovskite grains, multiple diffraction effects could not be avoided. Multiple diffraction gives rise to $0kl$ reflections with l = even and k = odd and $h00$ reflections with h = even that violate the extinction conditions for the 2_1 screw axis along **a***. Other reflections forbidden by space group extinctions are produced by twinning on the normal to (121) (illustrated schematically in Fig. 4). The major effect of the twin operation is to produce systematic rows of diffraction spots in SAED patterns at ½ $0kl$ where k is even and l is odd (Fig. 4). Although the actual twin operation is a twofold rotation around [121], it has the appearance of a 120° rotation around [012] (the pseudocubic [111]). In finely twinned crystals, the SAED patterns show that up to three orientations of twin-related domains are generating the observed diffraction effects (Fig. 5).

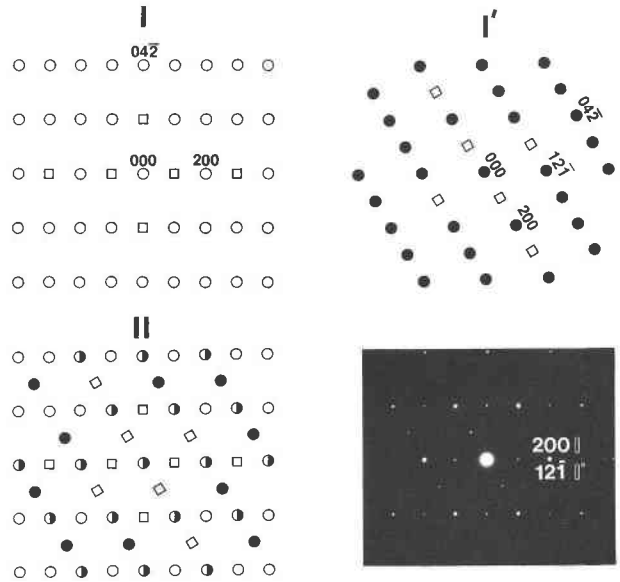

Fig. 4. Schematic diffraction patterns for the [012] zone, illustrating the twinning operation on the normal to (121). Combining patterns I and I' generates pattern II, which corresponds to the experimental SAED pattern.

Figure 6 is an HRTEM image of the interface between two twin-related domains. The (100) planes (0.54-nm periodicity in the image) meet at an angle of ~120°. The lack of strain contrast at the boundary between twins suggests that there is minimal disruption of the structure. TEM images indicate that the boundaries between twins are irregular and complicated by overlap in thick regions of the sample (Fig. 7), although lamellar (121) twins also occur. The HRTEM images indicate that the composition plane between twins is inclined to the [012] zone axis.

The 180° rotation twin around [101]

Twins of this type are impossible to recognize in [101] SAED patterns because of the superposition of the diffraction spots (i.e., pseudomerohedral twinning). White et al. (1985) documented this type of twinning using high-

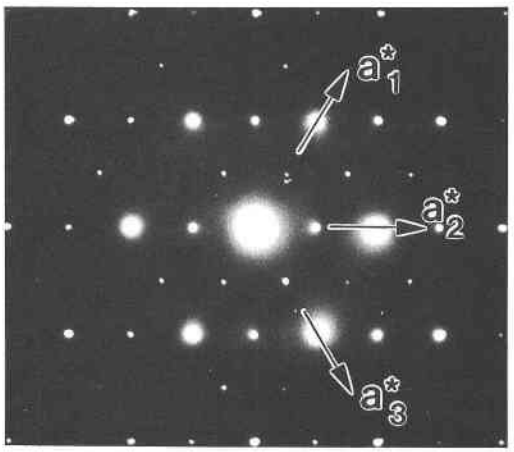

Fig. 5. SAED pattern of the [012] zone showing three orientations (subscripts 1, 2, and 3) of **a*** in a finely twinned region. Compare with Figs. 3 and 4.

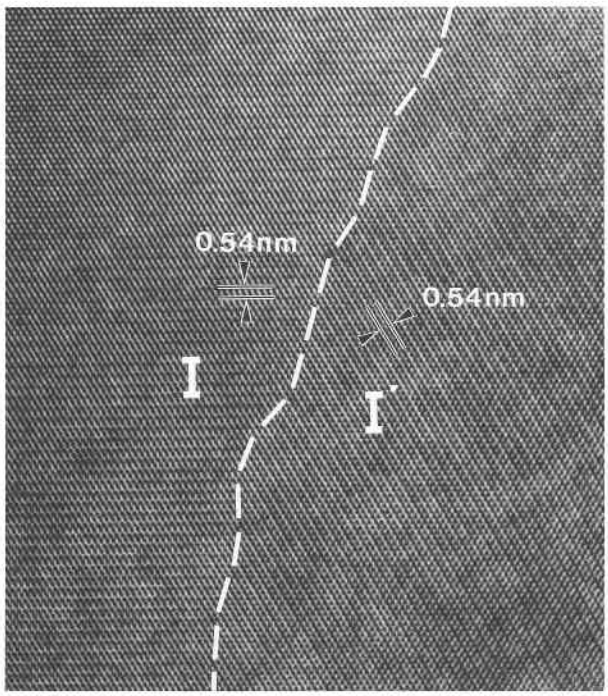

Fig. 6. HRTEM image of the interface between (121) twins (I and I'). The interface is essentially free of strain and is highly irregular, suggesting that the composition plane is inclined to the zone axis.

resolution TEM images from the [101] zone axis. They observed lamellar defects parallel to the **b** axis, which they interpreted as the composition plane between two twin domains. We found that twinning by a rotation of 180° around [101] can also be identified from zone axes other than [101]. For example, SAED patterns from [100] contain $0k0$ reflections with k = odd and $0kl$ reflections with k = odd and l = even; these are forbidden by space group extinctions (specifically, they violate the extinctions for the 2_1 screw axis along **b*** and the n glide). These reflections do not result from multiple diffraction; however, the reflections can be generated if a twin operation occurs such that [001] and [100] zones are intergrown and in a twin relationship. The composite SAED pattern that results from a crystal that has undergone this type of twinning is shown schematically in Figure 8. In the experimental SAED pattern it should be noted that [001] and [100] are not exactly coincident (as shown by the asymmetrical distribution of diffraction intensities around the central spot), but they are displaced from one another by ~0.5°. The [100] zone of orthorhombic perovskite is equivalent to the [110] zone in the pseudocubic cell.

HRTEM images from [100] of perovskite show strong (011) lattice fringes (0.44 nm) and a 0.38-nm (020) spacing along **b** (Fig. 9). HRTEM images from the [001] zone contain regions with a 0.76-nm periodicity along **b** (Fig. 9). Optical diffraction patterns indicate an intergrowth of [100] and [001] twin domains. The twin boundaries are abrupt but irregular, indicating that the composition plane is a higher order plane or a composite of several interfaces. We have also observed rare lamellar twins with (010) as the composition plane.

Discussion

Perovskite in the refractory inclusions in meteorites possessed cubic symmetry at the high temperatures (~1650–1500 K) estimated for its formation (Grossman and Larimer, 1974). On cooling, perovskite undergoes a displacive phase transition from high symmetry (cubic) to lower symmetry orthorhombic. The fact that twinning on the normal to (121) is so seldom observed in terrestrial end-member perovskite may be related to the temperature of formation, the rapidity of quenching, and the rarity of end-member perovskite in terrestrial rocks. The majority of terrestrial rocks that contain perovskite formed at temperatures below the cubic-orthorhombic transition temperature. For the few occurrences where the temperatures exceeded the transition temperature, the cooling rates were slow enough to destroy the (121) twins by annealing. In order to test this hypothesis, we performed experiments using synthetic perovskite heated to high temperature, followed by variable quench rates. Our cooling-rate experiments are semiquantitative but indicate that (121) twins are common only in the fast cooling-rate experiments (≥50 °C/min), whereas in the slow cooling-rate experiments (≤50 °C/min), (101) twins predominate. A similar result was obtained in experiments by Wang et al. (1992) on terrestrial perovskite, which showed that (121) twins were dominant only in crystals quenched from 1693 K. If these experiments can be directly compared with the meteoritic perovskite, the results indicate that the meteoritic perovskite displaying (121) twins was not only heated to high temperatures (>1573 K) but was also quenched rapidly.

Twinning in perovskite can also result from deformation processes, and many CAIs show petrographic evidence for deformation (mainly kink bands in gehlenite).

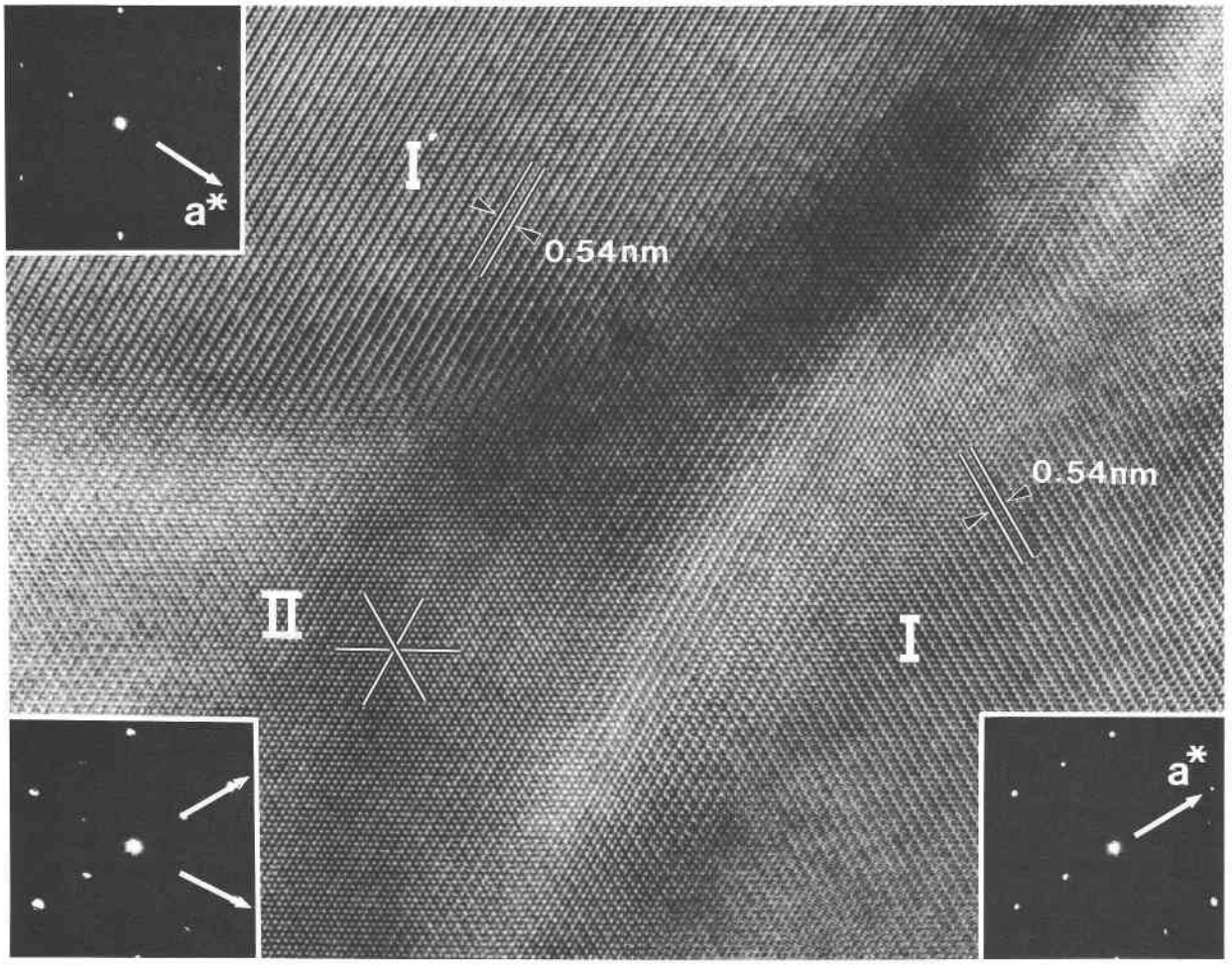

Fig. 7. HRTEM image of (121) twins viewed down [012]. Regions I and I′ are individual twins separated by region II, where they overlap. Insets are optical diffraction patterns showing the orientation of **a*** in each region.

However, several studies have shown that the deformation of perovskite results in the formation of predominantly (101) twins (Doukhan and Doukhan, 1986; Wang et al., 1992). Thus, we conclude that the microtwinning results from the unusual thermal history of these perovskite samples. The microtwinning and, in particular, the (121) twins probably formed during crystal growth in the stability field of cubic perovskite, or during the transition from cubic to lower symmetry on cooling.

The constraints of flash heating, imposed by petrographic and trace-element data (Wark et al., 1988), coupled with rapid cooling deduced from the cooling-rate experiments, place limits on the processes involved in the

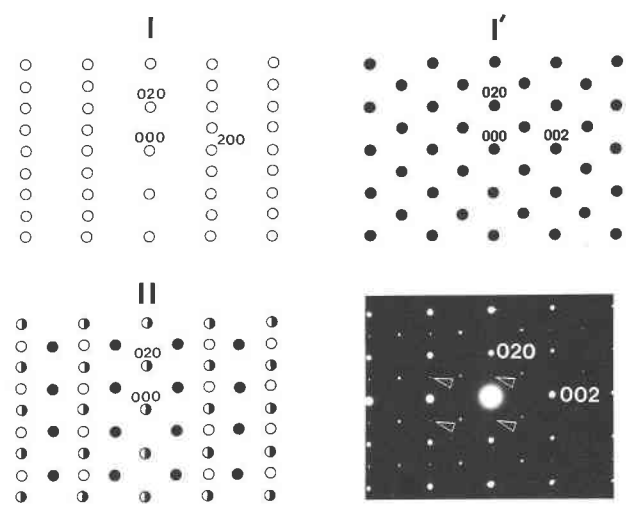

Fig. 8. Schematic and selected-area electron diffraction (SAED) patterns for the [100] zone (I) and [001] zone (I′) of perovskite. Examples of the reflections from the [001] zone are indicated by arrows. Combining patterns I and I′ generates pattern II, which corresponds directly to the experimental SAED pattern.

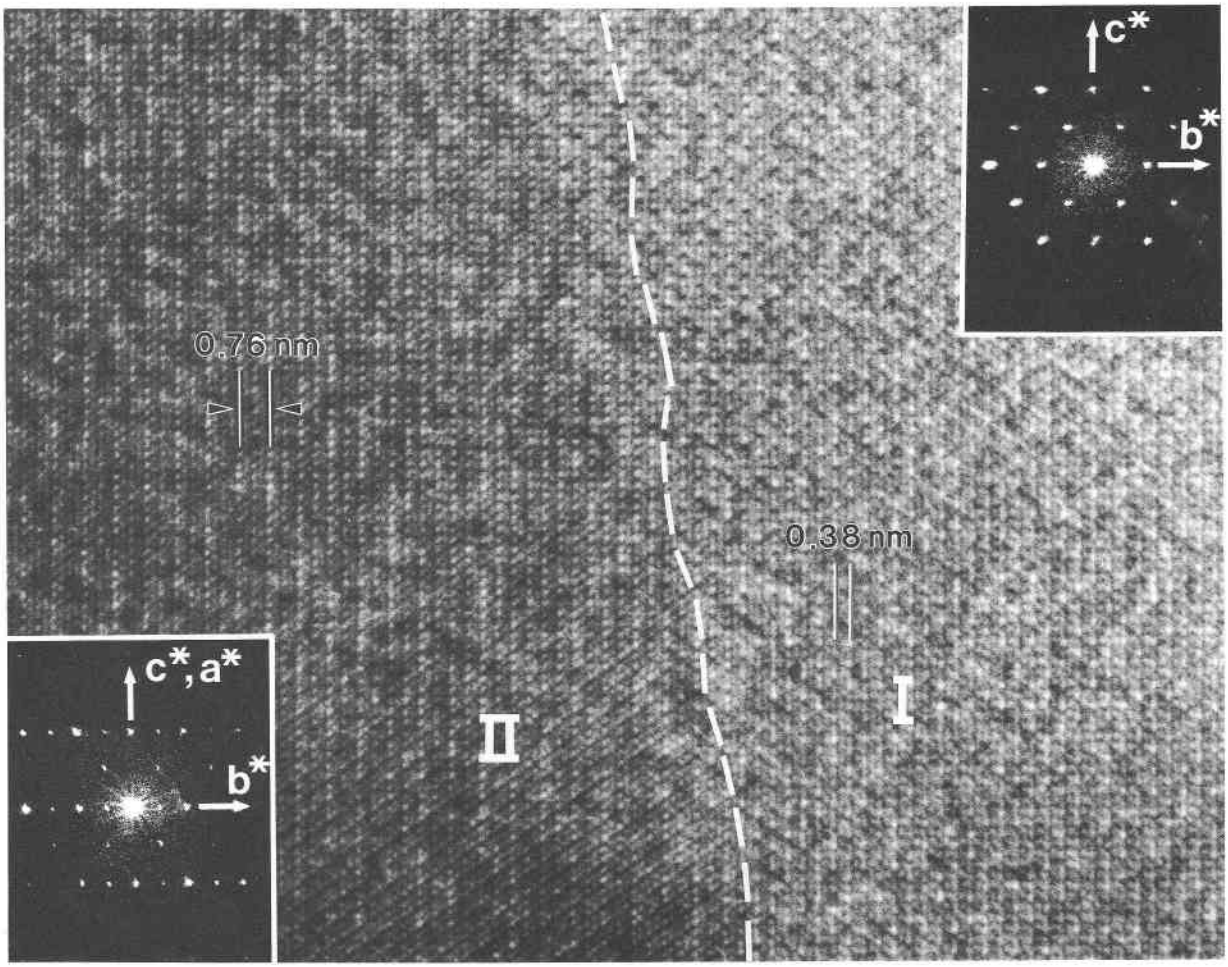

Fig. 9. HRTEM image of perovskite viewed down [100]. The dashed line separates a region of normal perovskite (I) from a twinned region (II). The inserts are optical diffraction (OD) patterns. The OD pattern in region II shows reflections from both [100] and [001] zones that are in a twin relationship (compare with Fig. 8).

formation of refractory rims on CAIs. Murrell and Burnett (1987) summarized potential mechanisms for the formation of refractory rims including formation by (1) deceleration heating in parent body atmospheres, (2) deceleration heating in nonuniform gas densities in the solar nebula, (3) flash heating during transit through nebular hot spots, (4) differential sublimation of CAI melts, (5) direct condensation, and (6) recondensation of vaporized material. Option 4 can be eliminated because crystallization times are so long for molten CAIs ($<10^6$ s, Stolper and Paque, 1986) that significant annealing of the perovskite is to be expected. Options 5 and 6 invoke condensation processes and also have difficulties accounting for fast cooling because of the evidence for a continuous series of gas-solid reactions extending down to ~400 K in altered CAIs (Hashimoto and Grossman, 1987; Keller and Buseck, 1991). Options 1–3 satisfy the criteria for flash heating and cooling, but options 2 and 3 should produce rim sequences of varying thicknesses, depending on the size of the hot spots or gas density fluctuations, whereas the petrographic evidence indicates that rim sequences are generally of relatively constant thickness. Thus, of these six options, we believe from crystallographic and petrographic observations that option 1 best satisfies the criteria. An additional possibility not considered by Murrell and Burnett is that these refractory rims could result from primordial lightning in the solar nebula. It has been shown that lightning can provide the requisite flash heating and also has the characteristic of rapid cooling (Eisenhour and Buseck, 1993), but experiments in appropriate starting materials are required to evaluate this process fully.

Acknowledgments

This work was supported by NASA grant NAG 9-59. Samples of Allende CAIs were provided by C.B. Moore and C. Lewis at the Center for Meteorite Studies at Arizona State University, and Vigarano samples were provided by G. MacPherson at the Smithsonian Institution. Special thanks go to G. Lofgren for running the cooling-rate experiments in the Experimental Petrology Labs at NASA–Johnson Space Center. We thank R. Sharma for assistance with the JEOL 4000EX. D. Eisenhour and F. Allen

are thanked for helpful discussions. Reviews by A. Brearley and M. Murrell are appreciated. Electron microscopy was performed at the Facility for High Resolution Electron Microscopy in the Center for Solid State Science at ASU, established with support from the National Science Foundation (NSF) grant no. DMR-86-11609 and at the Electron Beam Analysis Laboratories at the NASA–Johnson Space Center.

REFERENCES CITED

Boynton, W.V., and Wark, D.A. (1987) Origin of CAI rims. I. The evidence from the rare earth elements. Lunar and Planetary Science Conference, 18, 117–118.

Doukhan, N., and Doukhan, J.C. (1986) Dislocations in perovskites $BaTiO_3$ and $CaTiO_3$. Physics and Chemistry of Minerals, 13, 403–410.

Eisenhour, D., and Buseck, P.R. (1993) Primordial lightning: Evidence preserved in chondrites. Lunar and Planetary Science Conference, 24, 435–436.

Grossman, L. (1980) Refractory inclusions in the Allende meteorite. Annual Reviews of Earth and Planetary Science, 8, 559–608.

Grossman, L., and Larimer, J.W. (1974) Early chemical history of the solar system. Reviews of Geophysics and Space Physics, 12, 71–101.

Hashimoto, A., and Grossman, L. (1987) Alteration of Al-rich inclusions inside amoeboid olivine aggregates in the Allende meteorite. Geochimica et Cosmochimica Acta, 51, 1685–1704.

Hu, M., Wenk, H.-R., and Sinitsyna, D. (1992) Microstructures in natural perovskites. American Mineralogist, 77, 359–373.

Kay, H.F., and Bailey, P.C. (1957) Structure and properties of $CaTiO_3$. Acta Crystallographica, 10, 219–226.

Keller, L.P., and Buseck, P.R. (1991) Calcic micas in the Allende meteorite: Evidence for hydration reactions in the early solar nebula. Science, 252, 946–949.

Liebermann, R.C., Wang, Y., and Liu, X. (1990) Domain structure and phase transitions in $CaTiO_3$ perovskite at high temperature (abs.). Eos, 71, 529.

Liu, X., and Liebermann, R.C. (1988) $A^{2+}B^{4+}O_3$ perovskites at high temperature (abs.). Eos, 69, 1451.

Megaw, H.D. (1973) Crystal structures: A working approach, 563 p. Saunders, Philadelphia.

Müller, O., and Roy, R. (1974) The major ternary structural families, 487 p. Springer-Verlag, New York.

Murrell, M.T., and Burnett, D.S. (1987) Actinide chemistry in Allende Ca-Al-rich inclusions. Geochimica et Cosmochimica Acta, 51, 985–999.

Newnham, R.E. (1987) Structure-property relationships in perovskite electroceramics. In A. Navrotsky and D.J. Weidner, Eds., Perovskite: A structure of great interest to geophysics and materials science. American Geophysical Union Monograph, 45, 91–98.

Sasaki, S., Prewitt, C.T., and Bass, J.D. (1987) Orthorhombic perovskite $CaTiO_3$ and $CdTiO_3$: Structure and space group. Acta Crystallographica, C43, 1668–1674.

Stolper, E., and Paque, J.M. (1986) Crystallization sequences of Ca-Al-rich inclusions from Allende: The effects of cooling rate and maximum temperature. Geochimica et Cosmochimica Acta, 50, 1785–1806.

Wang, Y., Guyot, F., and Liebermann, R.C. (1992) Electron microscopy of (Mg, Fe)SiO_3 perovskite: Evidence for structural phase transitions and implications for the lower mantle. Journal of Geophysical Research, 97, 12327–12347.

Wark, D.A., Spettel, B., Palme, H., and El Goresy, A. (1988) Rim formation by flash heating and metasomatism: Evidence from Vigarano CAI VI-1. Lunar and Planetary Science Conference, 19, 1230–1231.

Williams, Q., Knittle, E., and Jeanloz, R. (1987) Geophysical and crystal chemical significance of (Mg, Fe)SiO_3 perovskite. In A. Navrotsky and D.J. Weidner, Eds., Perovskite: A structure of great interest to geophysics and materials science. American Geophysical Union Monograph, 45, 1–12.

White, T.J., Segall, R.L., Barry, J.C., and Hutchison, J.L. (1985) Twin boundaries in perovskite. Acta Crystallographica, B41, 93–98.

MANUSCRIPT RECEIVED APRIL 5, 1993
MANUSCRIPT ACCEPTED SEPTEMBER 27, 1993